Featured in Physics

Foot function enabled by human walking dynamics

Daniel Renjewski *
Chair of Applied Mechanics, Department of Mechanical Engineering, School of Engineering and Design, TU Munich, 85748 Garching, Germany

Susanne Lipfert
Section for Applied Sport Science, Department of Sport and Health Sciences, TU Munich, 80809 München, Germany

Michael Günther
Computational Biophysics and Biorobotics Group, Institute for Modelling and Simulation of Biomechanical Systems, University of Stuttgart, 70569 Stuttgart, Germany

(Received 6 May 2022; accepted 23 October 2022; published 8 December 2022)

Bipedal walking, the habitual gait for man, is rather unique in nature and poses particular challenges for balance and propulsion. The characteristic double-humped ground reaction force profile has been widely observed but not put into functional context. We propose a mathematical model that captures the dynamics of the human foot in walking including the characteristic motion of the center of pressure. Using this model, we analyze the functional interplay of all essential biomechanical contributors to foot dynamics in walking. Our results demonstrate the intricate interplay of a self-stabilizing mechanism which allows extending a leg's stance phase while simultaneously powering rapid swing by condensing the essentials of foot dynamics into a reductionist, biomechanical model. A theory is presented which identifies the foot to be the key functional element and which explains the global dynamics of human walking. The provided insights will impact gait therapy and rehabilitation, the development of assistive devices, such as leg prostheses and exoskeletons, and provide guidelines for the design and control of versatile humanoid robots.

DOI: 10.1103/PhysRevE.106.064405

I. INTRODUCTION

Humans are the only habitual bipedal *distance* walkers among mammals [1] with markedly double-humped force patterns [2]. Moving on two legs comes with specific challenges concerning balance, support, and propulsion, which results in peculiar dynamics aimed at reconciling two competing objectives: To enhance controllability by extended stance phase duration [3,4] and, as a consequence of the resulting high duty factor, to recirculate inert legs in the brief remainder of the gait cycle (GC).

For humans, walking is more efficient than running, even at optimal speeds [5]. The characteristic force pattern of running is governed by the natural frequency of the leg [6]. As this frequency cannot be reduced arbitrarily, walking seems to be achieved by increasing the natural frequency—the leg stiffness is reported to increase for walking in comparison to running [7]—while reducing the mechanical energy fluctuations to keep the leg on the ground for two periods instead of one. Accordingly, the force pattern each leg experiences over the course of a stance phase is double-humped. This fundamental frequency modulation of the leg-axis mode, along with the further extension of single support through the forward motion of the center of pressure (CoP) by ankle plantarflexor loading, results in a long period of controllability while at the same time providing the power for rapid and efficient leg swing by means of a catapult mechanism. The importance of ankle plantarflexors for extending stance phase duration has long been experimentally observed [8].

The foot as a lever [1] plays a crucial role in allowing the CoP to shift for keeping a dynamic equilibrium while allowing the ankle plantarflexors to be loaded at the same time. Foot biomechanics has been extensively studied [9,10] by kinesiologists, orthopaedists, anthropologists, roboticists, and others. A number of key functions have been proposed which can be categorized into support and stability [9,11,12], increasing stride length and energy conversion [13–15], reducing the contact collision [16], and absorbing the impact by forceful plantarflexion [17,18].

The evolutionary development of the foot into a suitable lever for bipedal gait [1] has been postulated while a functional description tying this role to the observed global dynamics of human walking is lacking. So far, the foot's function in walking could not be explained from its structural complexity [19]. Moreover, the importance for Achilles tendon loading has not been acknowledged.

We present a mathematical model that explains foot dynamics in the sagittal plane with the foot in a crucial position as a lever for active forces reflected by the ground. Our model explains the benefit of the evolved, specifically human global gait dynamics. The resulting insights, elevating the foot's

*Daniel.Renjewski@tum.de

 ©2022 American Physical Society

function from a contacting body to a key functional element of human walking, substantially extend the understanding of human gait dynamics and will help to improve gait rehabilitation in patients as well as the design of better gait assistive devices and bio-inspired humanoid robots, which produce more efficient, versatile, and robust locomotion.

II. METHODS

Data collection and processing is described below. More detailed information is also available in Ref. [20]. In a nutshell, the way we came to our conclusions is to reduce mechanical complexity of the dynamics of the human foot by postulating a *time-invariant velocity pole*, which is indicative of a pure rotational motion (Fig. 3), and confirming it based on experimental data (Sec. II B 2). This allowed us to write down a single, scalar equation of motion [Eq. ((3)] for the dynamic behavior of the foot in walking and analyze it comprehensively using data acquired from human walking trials. Formulating expressions for the core interplay of primary foot drivers, i.e., ankle force and ankle torque, and the characteristic shift of the CoP (Sec. B 1) allowed us to identify fundamental connections between global walking dynamics and foot function, reflected in the relation between the two foot drivers. We further determined key events in the gait cycle of human walking (see Appendix C for a detailed description of events) and identified their temporal and dynamic relations to gain further functional insight.

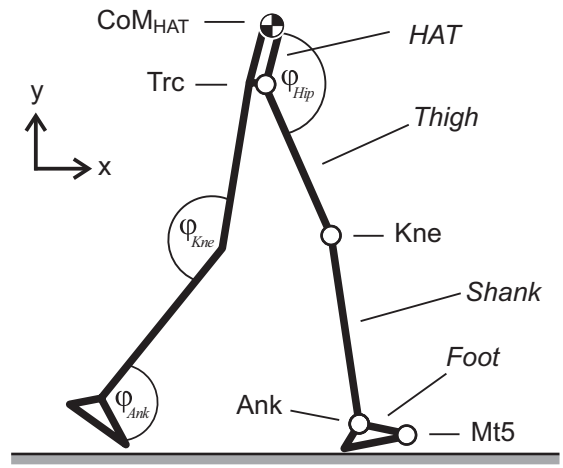

FIG. 1. Kinematic setup. Sagittal marker positions were recorded at the hip (greater trochanter, Trc), the knee (lateral knee joint gap, Kne), the toe (5th metatarsal joint, Mt5), and the ankle (lateral malleolus, Ank). The center of mass (CoM) of the HAT segment was derived from sex-, height-, and weight-specific regression curves [22]. The foot segment was defined between Mt5 and Ank, the shank segment between Ank and Kne, the thigh segment between Kne and Trc, and the HAT segment between Trc and $\mathrm{CoM_{HAT}}$. Ankle angle φ_{Ank}, knee angle φ_{Kne}, and hip angle φ_{Hip}, were defined as inner joint angles between two adjacent segments.

A. Data collection

We used experimental data from Ref. [21], in which three-dimensional (3D) lower limb kinematics and ground reaction forces (GRF) were collected from 21 subjects (11 females, 10 males) walking at 75% of their preferred transition speed between walking and running (approximately 1.5 m s^{-1}) on an instrumented treadmill (type ADAL-WR, HEF Tecmachine, Andrezieux Boutheon, France). The study was approved by the University of Jena Ethics Committee (in accordance with the Declaration of Helsinki) and written informed consent was provided by all subjects prior to the experiments. Subjects wore athletic footwear in which they felt comfortable and were given ample time for warming up and getting familiar with the treadmill. None of the participants reported any case of locomotor deficit.

Motion analysis was performed using eight wall-mounted high-speed infrared cameras (Qualisys, Gothenburg, Sweden) recording at a sampling frequency of 240 Hz. For the present study, we used camera recordings of the sagittal positions of eight reflective markers placed over anatomical landmarks of both of the subject's lower limbs (Fig. 1), respectively. The center of mass of the head-arms-trunk (HAT) segment ($\mathrm{CoM_{HAT}}$) was derived from sex-, height-, and weight-specific regression curves from Refs. [22] and [[23], p. 62ff]. Ground reaction forces (GRFs) were recorded at a frequency of 1000 Hz and down-sampled to 240 Hz.

Kinematic and GRF data were recorded simultaneously, synchronized by a trigger signal provided by the treadmill computer. The remaining time delay (2.5×10^{-3} s) and time drift (2.0×10^{-5} s s^{-1}) between both systems were identified and corrected after the measurements [24].

B. Data processing

Initially, an inverse dynamics procedure [[25], Sec. 2.1], including digital filtering and marker processing [[26], Appendix], was performed. Leg joint torques and forces can be calculated implementing inverse dynamics algorithms. Inconsistencies between inverse dynamics model assumptions (e.g., rigid segments) and measured kinematics (e.g., fluctuating segment lengths due to skin marker movement) can be identified and corrected. In our analysis, raw skin marker trajectories were processed such that constant segment lengths throughout measured sequences were guaranteed (see Ref. [[26], Appendix] for further details) before calculating inverse dynamics. Essentially, we determined sagittal ankle, knee and hip joint torques for each leg by a sequential algorithm [25] based on the sagittal coordinates of four markers per leg (Fig. 1). After having digitally filtered and processed the marker positions, and calculated their first and second derivatives, the equations of motion of a leg's chain of segments were solved at each sample, from distal to proximal and independently for each leg, for the (three) sagittal components of the joint force (two) and torque (one), taking soft tissue dynamics into account [25].

All data were then processed and analyzed using custom software (MATLAB R2007b-2021a, MathWorks, Inc., Natick, MA). Signals of detected gait cycles (starting at touchdown of one leg and ending with the next touchdown of the same leg) were linearly interpolated to 201 samples and then averaged at each sample (implicit time-normalization) for each subject to give individual means (left and right side

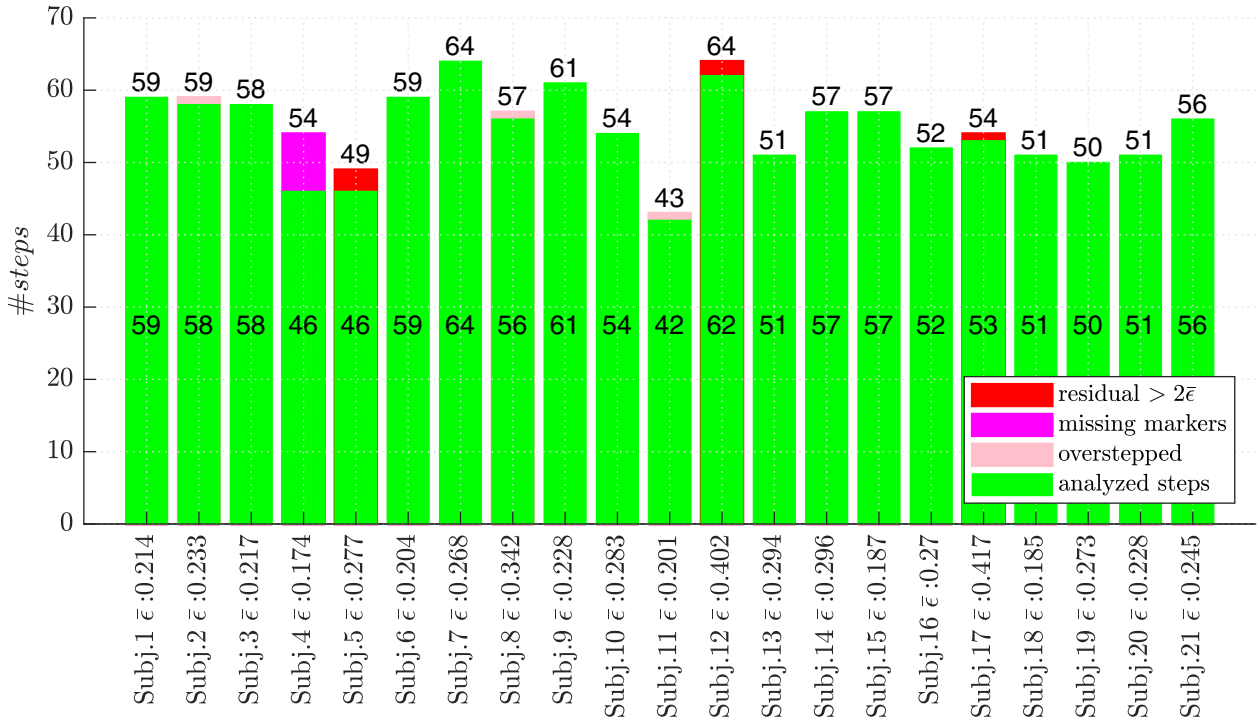

FIG. 2. Evaluated and discarded steps per subject. Bars indicate the number of recorded steps per subject with the total number of recorded steps listed above each bar. Colors indicate evaluated and discarded steps (see legend). The average residual (in Nm) of a function fit to the foot acceleration signal (see Appendix B 4 for fitting details) is listed for each subject.

combined). At 75% preferred transition speed, 1160 steps were collected. In total, we analyzed 1143 (see Sec. II B 1) walking gait cycles (between 42 and 62 per subject, Fig. 2). Definitions of sagittal plane kinematics are illustrated in Fig. 1. The collected marker trajectories were used to define foot, shank, thigh and HAT segments. Joint angles at the ankle (φ_{Ank}) were measured between the corresponding two adjacent segments and were defined to increase with joint extension. Angular velocity $\dot{\varphi}$, acceleration $\ddot{\varphi}$ and jerk $\dddot{\varphi}$ were derived using a central difference approximation: a moving average with a centered window of size 9 including four previous data points (causal) and four following data points (noncausal) each time a derivative is calculated. All kinematic and force plate data (force and CoP components) were low-pass filtered using a zero-lag second-order Butterworth filter with a cutoff frequency of 40 Hz [27].

1. Discarded steps

From the entirety of all experimentally collected step data, few had to be discarded for one of three reasons (Fig. 2). On the one hand, there were a number of steps for which markers were lost during the experiment and thus key dynamic properties could not be calculated due to the marker kinematics already missing before data processing. On the other hand, few steps turned out to show large deviations in their dynamics, determined by foot torque fit residuals (see Appendix B 4 for fitting details) exceeding two times the mean residual for the respective subject, which were also not considered for this study. Finally, for a number of steps the subject overstepped the boundary between left and right force plates and thus dynamics could not be properly separated in double support. In summary, 1143 of the 1160 recorded steps were left to be analyzed, which amounts to an average of (54 ± 5) steps per subject.

2. Single point of rotation

The authors make the assumption that the foot, while deforming during stance and rolling over its ball after the heel left the ground, still executes a pure rotation about a single point (a time-invariant velocity pole), which is to be determined. This rotation is characterized by constant vector lengths between this point of rotation and at least two landmarks of the foot throughout a defined time interval. The two chosen landmarks are ankle marker and the foot's kinematically determined CoM. The deviation $d(t)$ from the assumed constant vector length can be expressed as

$$d_{\text{CoM},f}(t) = R_{\text{CoM},f} - \sqrt{(x_{\text{CoM},f} - x_c)^2 + (y_{\text{CoM},f} - y_c)^2},$$
$$d_{\text{Ank}}(t) = R_{\text{Ank}} - \sqrt{(x_{\text{Ank}} - x_c)^2 + (y_{\text{Ank}} - y_c)^2}, \qquad (1)$$

where $R_{\text{CoM},f}$ and R_{Ank} are the time-invariant Euclidian distances between the point of rotation and the foot's center of mass and the ankle, respectively, $(x_{\text{CoM},f}, y_{\text{CoM},f})$ and $(x_{\text{Ank}}, y_{\text{Ank}})$ are the time-variant positions of the respective landmarks, and (x_c, y_c) are the coordinates of the time-invariant point of rotation. As landmarks, the experimentally measured position of the ankle joint marker as well as the position of the foot's center of mass are used, the latter being determined in post-processing from markers on the ankle and metatarsal joints. An optimization problem has been formulated to determine R_{Ank}, $R_{\text{CoM},f}$, x_c, and y_c by means of

Eq. (1) as

$$\underset{R_{\mathrm{Ank}},R_{\mathrm{CoM}f},x_c,y_c}{\mathrm{argmin}} \sum_t |d_{\mathrm{Ank}}(t)\, d_{\mathrm{CoM}f}(t)| \tag{2}$$

and solved using *lsqnonlin* in Matlab2020b (Mathworks, Natick, MA) for each experimental step individually. The time interval of the optimization is set to start with the instant the heel initiates movement to leave the ground, determined by the last sample at which the vertical ankle velocity (calculated by differentiation of the experimentally recorded vertical ankle marker position using Matlab's gradient function) is below a threshold of $1 \times 10^{-3}\mathrm{ms}^{-1}$, and ends three samples before the foot leaves the ground as experimentally determined by the disappearance of the measured vertical GRF component. A video explaining the general assumptions for our model may be found in the Supplemental Material [28].

C. Evaluation

For the entire optimization period the deviation in percent of the instantaneous vector length ($|\vec{R}_{\mathrm{CoM},f}|$ and $|\vec{R}_{\mathrm{Ank}}|$), calculated with respect to the determined constant point of rotation (x_c, y_c), from the time-invariant Euclidean distances R_{Ank} and $R_{\mathrm{CoM},f}$, which result from the optimization, indicating the quality of our assumption (Fig. 4). In addition, given the residual motion of the foot while planted flat on the ground, we have also determined the percentage error for the extended period, starting with single support.

The existence of a time-invariant velocity pole allows for the introduction of mechanical assumptions, reducing the equations of motion from three to a single degree of freedom, scalar equation of motion [Eq. (3)]. The assumptions leading to and a detailed derivation of the equation of motion Eq. (3) are documented in Appendix B.

III. RESULTS

Our experimental analysis confirms that a single point of rotation during stance phase can be determined with a margin of error for constant lever arm length of less than 2% for the fitted data and less than 4% over most of the stance phase starting from the onset of single support (Fig. 4). Subjects exhibit different levels of left/right asymmetry resulting in two distinct CoR clusters for certain subjects. Subject #15 has been chosen as a representative subject to demonstrate the dynamic observations and consequences as the subject appears to be a good representation of the general dynamics. For comparison, the respective dynamics of all subjects are shown in Figs. 9 and 10. This finding yields the formulation of a one-dimensional mechanical model (Fig. 3) that describes the foot's sagittal plane dynamics and facilitates revealing its key function during stance in bipedal walking.

A. Dynamic observation

Two primary and independent mechanical drivers for the foot dynamics can be identified: the ankle torque component perpendicular to the sagittal plane ($\mathcal{T}_{\mathrm{Ank}}$), resulting from ankle plantarflexor loading, and the ankle force vector projected into the sagittal plane ($\vec{F}_{\mathrm{Ank}}$, with $|\vec{F}_{\mathrm{Ank}}|$ denoted as F_{Ank}) as a consequence of proximal body dynamics (Fig. 5). We derived

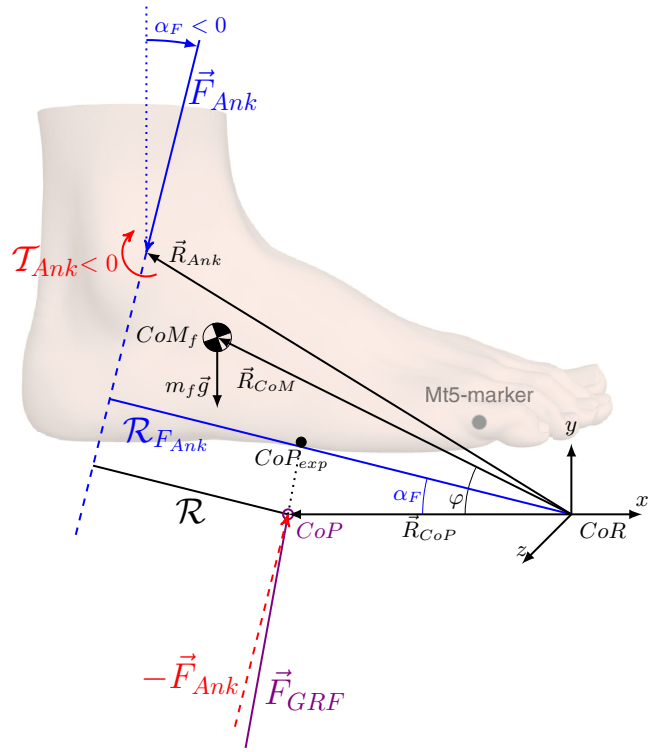

FIG. 3. A schematic of the foot model with all dynamic actors. The foot is assumed as a body defined by its center of mass CoM_f, its moment of inertia I_f and the location of the ankle joint. The marker at the 5th metatarsal joint (Mt5, see also Fig. 1) is used as a reference point on the foot (Fig. 4). The gravitational force $(0, -m_f\, g)^T$ acts on the center of mass, ankle force $\vec{F}_{\mathrm{Ank}}$ and ankle torque $\mathcal{T}_{\mathrm{Ank}}$ act at the ankle joint. The reflection of primary forces, i.e., the vector $\vec{F}_{\mathrm{GRF}}$ of the ground reaction force (GRF), acts on the foot at the position $\vec{R}_{\mathrm{CoP}} = (R_{\mathrm{CoP},x}, 0)^T$ of the moving center of pressure (CoP), which is the projection (see Sec. B 1) of the experimentally determined center of pressure ($\mathrm{CoP}_{\mathrm{exp}}$) along the instantaneous $\vec{F}_{\mathrm{GRF}}$ into the plane of the center of rotation (CoR). The positions of ankle, CoM_f and CoP relative to the CoR are given by the respective vectors. The symbol $\mathcal{R}$ indicates the lever for the resulting torque caused by the ankle force and its reflection. Subject to the resulting dynamics, the foot executes a pure tilt $(\dot{\varphi}, \ddot{\varphi})$ around the fixed CoR (Fig. 4).

the equation of motion for the foot [Eq. (3)] and grouped the drivers on the right-hand side into two key functional terms—a protagonistic torque term ($\mathcal{T}_{\mathrm{pro}}$), which rotates the foot toward takeoff, and an antagonistic torque term ($\mathcal{T}_{\mathrm{Ank}}$), which counters this tendency to keep the foot flat on the ground for an extended period of time (Fig. 6).

The protagonistic torque results from the ankle torque—governed by elastic tendon characteristics and isometric muscle operation [29]—and from the ankle force, which is reflected by the ground as a consequence of proximal body dynamics being transferred through the foot (Fig. 3). Each increase in ankle torque pushes the center of pressure (CoP) anteriorly [Eq. (B28)] and thus reduces the lever ($R_{\mathrm{CoP},x}$) of the reflected ankle force, which keeps the collective protagonistic torque contribution bound.

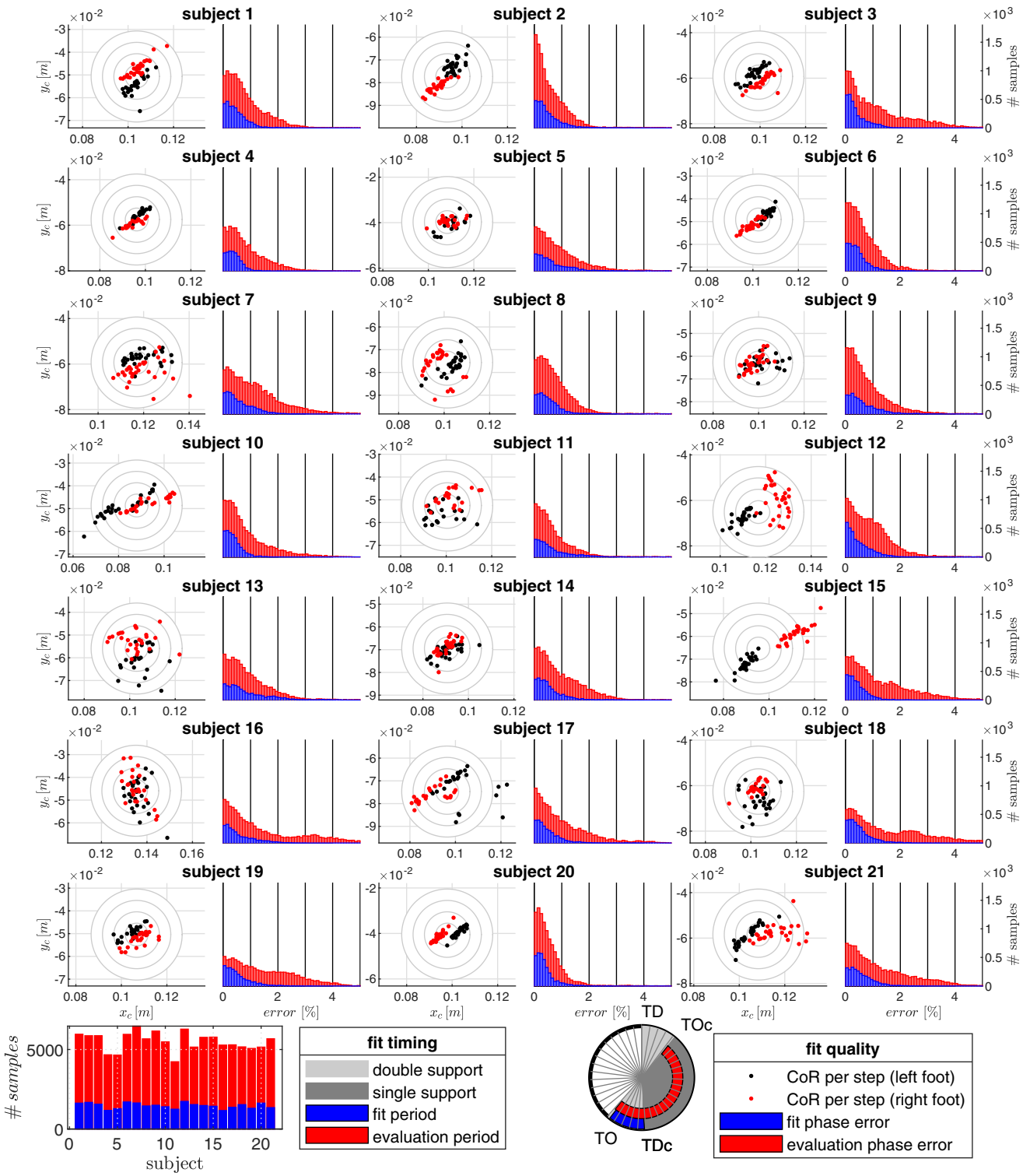

FIG. 4. CoR variability and lever length error. For each step, the position of the CoR (x_c, y_c, the origin of our model's coordinate system), determined by optimization (Appendix B 4), is indicated by a "+," given in coordinates relative to the ground (vertical) and the respective most anterior Mt5-marker (see Figs. 3 and 1) position while the foot is planted flat on the ground. CoRs for left and right steps are indicated individually as some subjects exhibit a clear left/right asymmetry, resulting in CoR clustering. Gray circles indicate a distance in steps of 5 mm from the median CoR of a subject respectively (2 cm for the outermost ring). Histograms show the number of samples for which each instantaneous lever arm $|\vec{R}_{\mathrm{CoM},f}|$ and $|\vec{R}_{\mathrm{Ank}}|$ deviates a certain percentage from its optimized fixed lever arm length $R_{\mathrm{CoM},f}$ or R_{Ank}, respectively. Each gray box indicates an error margin of one percent. Blue bars include only samples of the fit interval, red samples include the entire intervals beginning with the onset of single support and ending with the foot's takeoff. The bar graph at the bottom left indicates the total number of samples considered for either interval in each subject. The intervals are illustrated in the plot at the bottom right of the figure, with the full circle symbolizing an entire gait cycle.

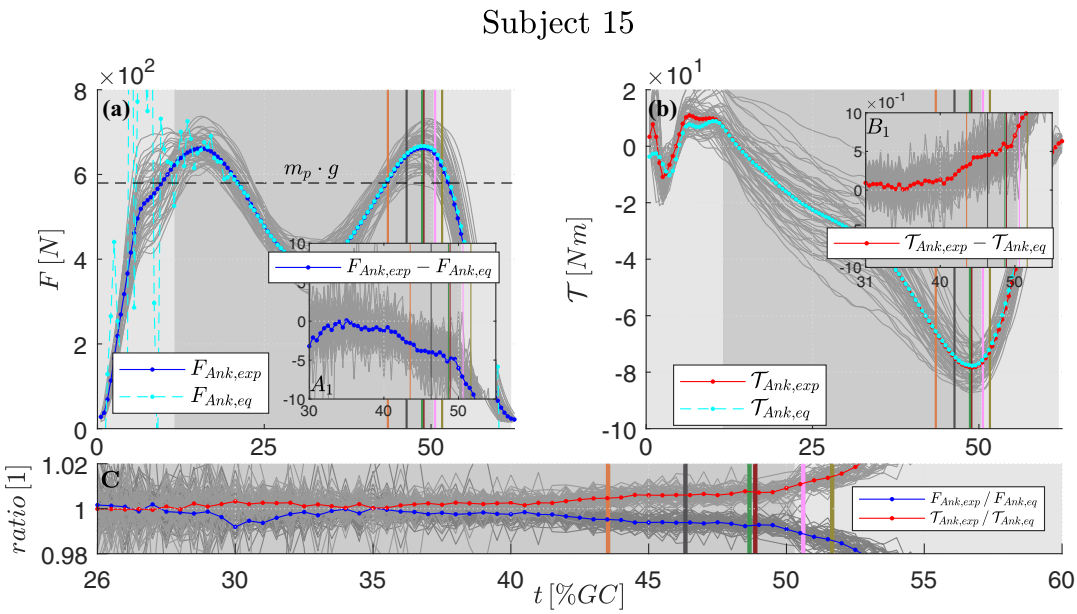

FIG. 5. Main actor dynamics during stance phase. The ankle force norm ($|\vec{F}_{\text{Ank}}| = F_{\text{Ank}}$), as determined by inverse dynamics, is shown in panel (A). The experimentally determined force ($F_{\text{Ank,exp}}$) for each step is shown in dark gray, its mean is shown in blue, and the corresponding equilibrium force ($F_{\text{Ank,eq}}$), calculated from Eq. (3) with the left-hand side set to zero is depicted as a dashed cyan line. The dashed black line indicates the combined weight of all segments proximal to the foot on the ground ($m_p\,g$). *Gray shadings of the background indicate single support (dark) and double support (light).* Panel (A_1) shows the difference of both signals. The vertical lines indicate important gait events, namely averages of (i) the instance the ankle force exceeds $m_p\,g$ (orange), (ii) the instance the ankle power turns positive indicating the onset of push-off and alleviation phase [26] (gray), (iii) the instance the ankle force reaches its second maximum (green), (iv) the instance the ankle torque reaches its minimum (brown), (v) the instance the trajectory of the resulting torque transitions into its bell-shaped part [(Fig. 8 in Appendix C), pink], and (vi) the onset of the launching phase defined by the jerk maximum of the ankle joint angle [26] (olive). The respective color for each event remains the same in all following figures. Analogously, in panel (B) the experimental ankle torque ($\mathcal{T}_{\text{Ank,exp}}$) is indicated in red, the equilibrium torque ($\mathcal{T}_{\text{Ank,eq}}$) in dashed cyan and panel (B_1) shows the difference of their norms. Panel (C) shows the relation of experimental and equilibrium force/torque in blue and red respectively over time, with 1 indicating equilibrium and values above 1 that the measured property exceeds the equilibrium torque. It can be clearly seen that force and torque depart from the equilibrium quite synchronously but in opposite directions indicating a loss of equilibrium in favor of the protagonist and forward rotation of the foot.

The antagonistic torque is a direct result of upper body dynamics, i.e., the weight and motion of all proximal segments, generating the resulting ankle force.

Torques caused by the foot's weight ($m_f\,g$) play a minor role ($\mathcal{T}_{\text{chg}}$, see Fig. 6). Due to the position of the foot's center of mass (CoM; mass: m_f), the torque of the foot's weight changes from protagonistic to antagonistic as soon as the forward traveling CoP at position $R_{\text{CoP},x}$ passes below the foot's horizontal CoM position $R_{\text{CoM},x}$, i.e., $\mathcal{R}_g = R_{\text{CoM},x} - R_{\text{CoP},x} = 0$ occurs [Eq. (3), Fig. 6(C)].

B. Dynamic consequences

According to the proposed equation of motion (Appendix B) that models the foot's rotational dynamics

$$\ddot{\varphi}\, I_{f,\text{CoR}} = \underbrace{-F_{\text{Ank}}\,\mathcal{R}_{F_{\text{Ank}}}}_{\text{antagonist}} - \underbrace{\mathcal{R}_g\, m_f\, g}_{\text{changing}} + \underbrace{\mathcal{T}_{\text{Ank}} - R_{\text{CoP},x}\, F_{\text{Ank},y}}_{\text{protagonist}}, \tag{3}$$

with $\ddot{\varphi}\, I_{f,\text{CoR}}$ symbolizing the foot's inertial torque, it becomes obvious that—as long as the ankle force ($\vec{F}_{\text{Ank}} = (F_{\text{Ank},x}, F_{\text{Ank},y})^T = F_{\text{Ank}}\,[\sin(\alpha_F), -\cos(\alpha_F)]^T$) is sufficiently large to counter the ankle torque $\mathcal{T}_{\text{Ank}}$ currently acting in the sagittal plane — the CoP will move to a position such that an equilibrium ($\ddot{\varphi} = 0$) arises, which keeps the foot stationary on the ground. With respect to the center of rotation (CoR, Fig. 3), the foot functions as a variable lever ($\vec{R}_{\text{CoP}} = (R_{\text{CoP},x}, R_{\text{CoP},y})^T$) for the ankle force reflected at the CoP, acting as a protagonist in concert with the ankle torque. The charging ankle force—the sole persistent antagonist—on the other hand, acts on a nearly constant lever arm (Fig. 3, $\mathcal{R}_{F_{\text{Ank}}} = R_{\text{Ank},x}\cos\alpha_F + R_{\text{Ank},y}\sin\alpha_F$), which varies only minutely with force direction (α_F). Both primary drivers, i.e., the ankle torque and the ankle force, reach their maximum magnitude close to the end of single support (Fig. 5), with the ankle torque ($\mathcal{T}_{\text{Ank}}$) peak marginally but consistently (within the uncertainty of one sample) succeeding the ankle force (F_{Ank}) peak (Fig. 8, fourth column, third row).

The resulting torque [Fig. 6(C)], i.e., the sum of antagonistic and protagonistic torque contributions, exhibits a consistent temporal characteristic expressed by a phase of near equilibrium followed by a bell-shaped peak which drives the rotation of the foot into takeoff. This characteristic can be modeled by the superposition of a linear and Gaussian function dependent on time (Appendix B 4). The onset of the bell-shaped curve follows the nearly concurrent extrema of

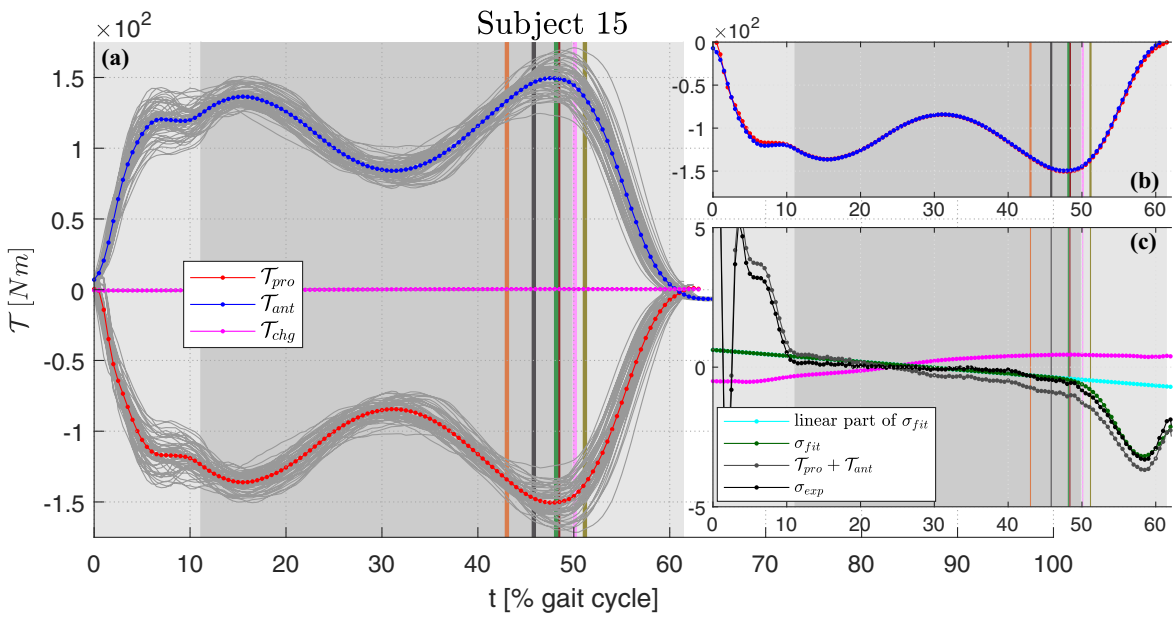

FIG. 6. Three torque contributions according to Eq. (3). Panel (A) shows the components of all individual steps in gray and means for antagonist ($\mathcal{T}_{\text{ant}}$), protagonist ($\mathcal{T}_{\text{pro}}$), and changing gravitational torque ($\mathcal{T}_{\text{chg}}$, very small in comparison). *Gray shadings of the background indicate single support (dark) and double support (light).* The vertical lines indicate averages of (i) the instance the ankle force exceeds $m_p\,g$ (orange), (ii) the instance the ankle power turns positive indicating the onset of push-off and alleviation phase [26] (gray), (iii) the instance the ankle force reaches its second maximum (green), (iv) the instance the ankle torque reaches its minimum (brown), (v) the instance the trajectory of the resulting torque transitions into its bell-shaped part [(see Fig. 8 in Appendix C) pink], and (vi) the onset of the launching phase defined by the jerk maximum of the ankle joint angle [26] (olive). Panel (B) shows a comparison of the protagonistic torque with the inverted antagonistic torque. Panel (C) shows the trajectory of the changing gravitational torque again, as well as the sum of torques ($\mathcal{T}_{\text{pro}} + \mathcal{T}_{\text{ant}}$) without the changing contribution. All three measured torque components (σ_{exp}), the linear part of the fit [Eq. (B29)], as well as the combined fit of linear and Gaussian parts [σ_{fit}, Eq. (B29)] are depicted (see Appendix B 4 for fitting details).

the primary drivers [$t_{\max}(F_{\text{Ank}})$, $t_{\min}(\mathcal{T}_{\text{Ank}})$; Figs. 6(C) and 8, columns 3–5]. Thus, the magnitude of the second hump in the ankle force trajectory determines the maximum ankle torque and hence the amount of elastic energy stored, while the timing of the peak in ankle force marks the release of the swing leg catapult.

C. CoP travel

Equation (3) can be solved for $R_{\text{CoP},x}$ (see Appendix B 3) to analyze the CoP's shift in position. The CoP consistently moves forward as a result of the increasing ankle torque but is kept on a dynamic equilibrium ($\ddot{\varphi}\, I_{f,\text{CoR}} = 0$) trajectory by the self-stabilizing ankle force lever as long as the counteracting force is sufficiently large (Fig. 7). As the force approaches saturation in late single support (Fig. 5), the CoP deviates from its equilibrium trajectory (Figs. 7 and 8). At the determined instance of loss of dynamic equilibrium [t_ϵ, (Appendix C)] the CoP deviation from its equilibrium position at this point in time amounts to (0.47 ± 0.33) mm. According to Eq. (B28), the CoP trajectory is determined by three main factors: The ankle torque, the magnitude of the ankle force, and the ankle force's direction.

D. Timing

The observed succession of events (Appendix C) during a gait cycle reveals the functional cascade leading to the loading and unloading of the ankle joint in human gait. Figure 6(A) shows the almost exactly mirrored trajectories of antagonistic and protagonistic actors as well as the very small contribution of the changing gravitational torque. During the first half of stance all three torques *nearly* cancel each other out and the foot remains firmly planted on the ground [Fig. 6(B)]. Approximately at midstance, when the ankle force approaches the minimum between both humps [Fig. 5(A)], the resulting torque slowly turns protagonistic [Fig. 6(C)]. During the final third of single support, the ankle force exceeds the combined weight of all proximal bodies [$m_p\,g$, Fig. 5(A)] and rises further toward its second peak which is reached briefly before the end of single support. In nearly instantaneous succession the ankle torque peaks as well. The period between both main drivers peaking is very brief with the ankle torque peak trailing the force peak in most cases (see Fig. 8, column 4, row 3). The resulting torque rapidly grows [Fig. 6(C)], causing an accelerated rotation of the foot through double support into swing.

IV. DISCUSSION

In human walking, a foot and the ground form a self-regulating mechanism during most of single support phase, which keeps the foot near static equilibrium. For a given magnitude of the ankle force, there is an upper limit to the magnitude of the ankle torque for which this equilibrium can be maintained. The corresponding CoP position results from the proportion of ankle force, in tandem with its reflection

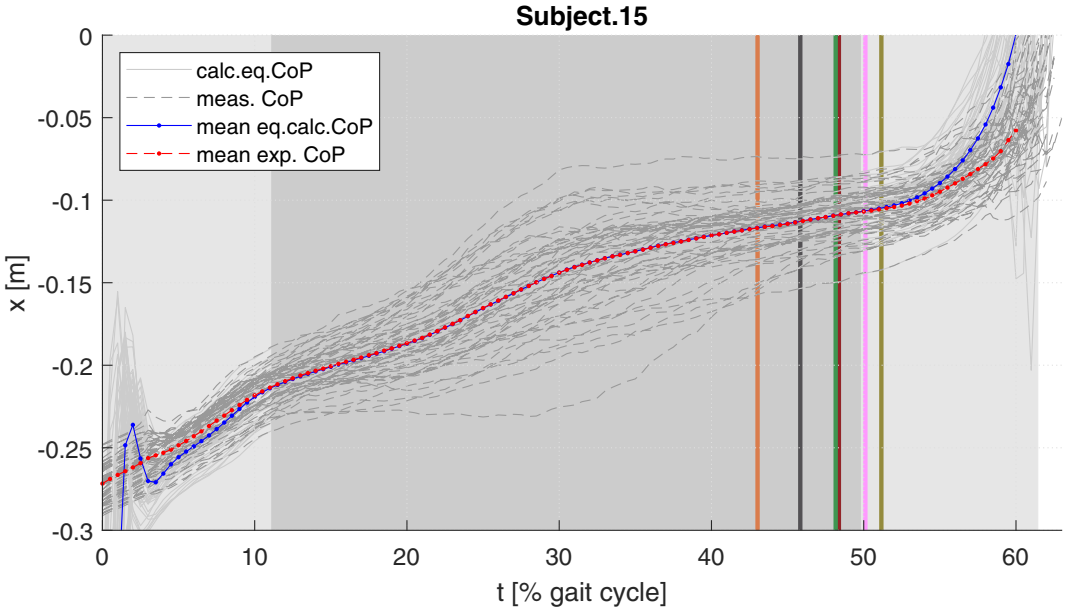

FIG. 7. Comparison of calculated and measured CoP progression. Gray lines indicate the CoP for each step, calculated for a dynamic foot equilibrium [$\ddot{\varphi}\, I_{f,\mathrm{CoR}} = 0$, Eqs. (B27) and (B28)] and compared to measured data. *Gray shadings of the background indicate single support (dark) and double support (light)*. Vertical colored lines indicate the timing of events as explained in the caption of Fig. 5 (see Appendix C for detailed description of events). In the instant when the equilibrium is lost (t_ϵ), the measured CoP deviates on average by (0.47 ± 0.33) mm from its equilibrium.

by the ground, and the ankle torque: An increasing torque moves the CoP anteriorly, whereas an increasing force generates the opposite. The observed monotonous forward motion of the CoP results from the ever increasing ankle torque. In the second half of single support, the foot ultimately creeps away from its dynamic equilibrium as a result of the weakening force rate succumbing to the ankle torque's sustained increase.

Importantly, because the ankle force is boosted by the proximal body dynamics, as seen in the force's second hump substantially exceeding proximal body weight ($m_p\, g$), the period of dynamic quasi-equilibrium is extended and the amount of elastic energy stored in the ankle plantarflexors increased. The stored energy compensates for the swing duration being diminished by the extended single support phase, through a powerful launch of the trailing leg into the subsequent swing during terminal stance.

Reductionist models of bipedal gait aim at explaining relevant fundamentals while omitting arguably less important details. We ponder established models from the viewpoint of characteristic frequency while also taking a look at the models' predicted walking dynamics.

The inverted pendulum model [30,31] is based on the observed arching trajectory of the whole body's CoM during midstance while in single support, but cannot reproduce the observed comprehensive walking pattern (phasing, dynamics) as, due to its single degree of freedom, it only exhibits a single gait frequency for a given speed and step length, i.e., the gait cycle itself with a single humped force trajectory for every stance phase.

In contrast, the spring-mass model [32] exhibits a wide range of possible characteristic frequencies tunable mainly by leg stiffness [6]. This range of frequencies allows a leg to maintain ground contact for consecutive periods producing the typical double-humped force profile observed in human walking. However, the analytical description of this double hump [2] suggests lower characteristic frequencies than the measured leg stiffness allows. Furthermore, the model predicts the force maxima to appear during double support phase, which indicates an additional dynamic mismatch. Thus, to synthesize humanlike gait, the extended contact time has to result fundamentally from two periods on the ground at a higher frequency which is determined by the superposition of gravitational acceleration, leg spring characteristics (stiffness and body mass), the system's state at touchdown [6,33], and finally the *shift of the center of pressure* which allows an extended near-equilibrium period due to the magnitude of the second force hump and cannot be reproduced by a single point of contact. High leg stiffness is in fact observed experimentally (Ref. [21], p.19, and Ref. [7], Table 2), but the lack of a foot illustrates a limitation of the originally proposed spring-mass model [6,32] for which even the longest stance duration predicted by the physiologically parameterized model is still substantially shorter than experimentally observed [[7], Fig. 5]. Interestingly, this frequency discrepancy in the model can be mitigated by adding a rolling foot [34], which increases the model's cycle time from 72% (without a foot) [7] to 102% [34] of experimentally observed cycle times [21]. In addition, the relation of gait frequency and speed in humans [[21], p. 56], namely a decrease in frequency at higher speeds, is inverse to the reported relation for the spring-mass model [[32], Fig. 4].

Apparently, another degree of freedom, namely the ankle joint, seems to be a key element to increase the stance duration, specifically by elongated single support [34]. Adding

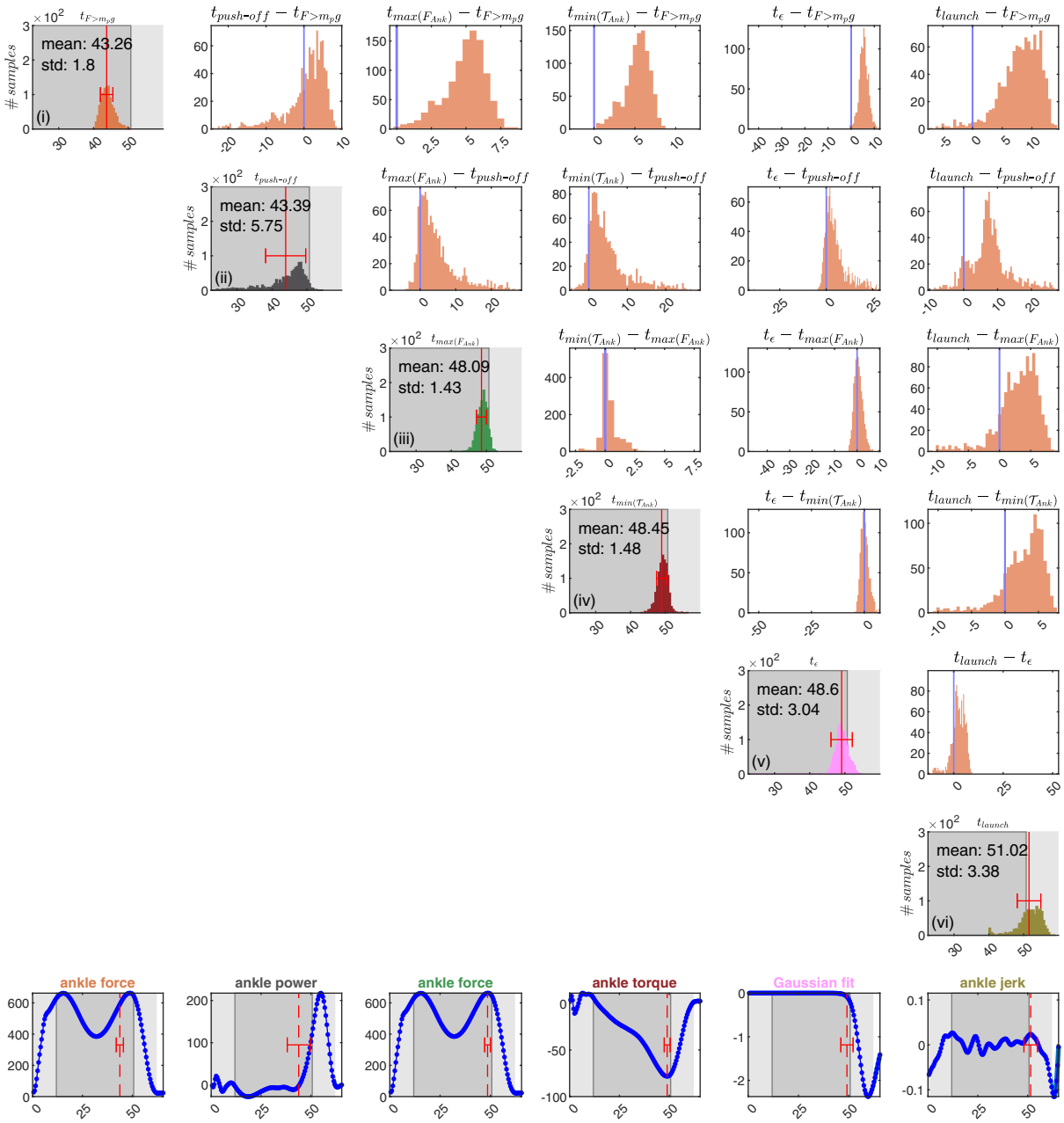

FIG. 8. Timing of important gait events. All histograms indicate the number of steps for which an event occurs at a specific sample, the x axis indicating time in % GC. Distribution of absolute event timing for all analyzed steps is shown on the diagonal. The events analyzed are (i) ankle force norm exceeds proximal body weight ($t_{F>m_pg}$), (ii) push-off onset ($t_{\text{push-off}}$), (iii) maximum of ankle force ($t_{\max(F_{\text{Ank}})}$), (iv) minimum of ankle torque ($t_{\min(\mathcal{T}_{\text{Ank}})}$), (v) loss of equilibrium (t_ϵ), and (vi) onset of launching phase [26] (t_{launch}). *Gray shading indicates single (dark) and double (light) support phases*. The touchdown of the contralateral leg (t_{TDc}, i.e., the right edge of the dark gray area occurs at (50.45 ± 0.16) % GC. The determination of all events is explained in detail in Appendix C. The mean event time (in % GC) and standard deviation are reported in numbers and indicated with a vertical line and horizontal error bar. The distribution of relative event timing is shown in the upper half for all analyzed steps. Each column shows the timing relative to all other key events as indicated in the subfigures' titles. Zero (marked with a blue vertical bar) indicates the number of steps for which the two events occur simultaneously; negative numbers indicate that the event of the respective row precedes the event of the respective column. The bottom row shows example trajectories of the respective characteristic quantities from which each event has been determined, with the mean event time indicated by a vertical dashed line and error bar.

this degree of freedom to the model without also imposing the appropriate dynamics by parameter adjustment cannot eliminate the temporal mismatch [[34], Fig. 5]. Fundamentally, to modulate the basic gait frequency for extending stance duration, given a limited range of possible leg stiffness, the axial and rotational dynamics of the segmented leg must act in concert. The interaction of the planted foot and the constraining ground provides the coupling mechanism for axial leg and rotational ankle dynamics, which makes it possible in effect to separate the characteristic axial and rotational frequencies and

therefore to mechanically decouple both degrees of freedom in the time domain. In other words, this mechanism allows the characteristic frequencies to be tuned by muscular actuation.

Our mathematical model [Eq. (3)] sheds light on this intricate dynamic interplay of leg force and ankle torque acting on the human foot. The combination of boosted leg force in the second hump and forward moving CoP due to increasing ankle torque, ultimately resulting in high-power launching of the swing leg, realises the required temporal parameters for an efficient, effortless, and sustainable bipedal gait.

Powering the leg swing from the ankle leads to a huge gain in efficiency. In fact, with respect to the hip being the leg's pivot point during the swing phase, the large mechanical advantage of the foot yields a clear efficiency benefit in contrast to hip flexors having a weak leverage as swing drivers [35–37]. Tuning leg stiffness through muscle action and exploiting the natural passive dynamics, in addition to being efficient, also substantially reduces control effort [38,39]. Moreover, rapid swing comes with additional advantages for swing leg controllability and passive gait stabilization in the terminal swing phase, e.g., through swing leg retraction [40,41]. This combination of low energy expenditure and low control effort makes walking an ideal endurance gait, which gave early humans an advantage in persistence hunting [5,42].

ACKNOWLEDGMENTS

This work was supported by the German Research Foundation (DFG) under Grants No. 449427815 and No. 234087184. S.L. conducted all experiments; S.L., M.G., and D.R. analyzed the biomechanics data; D.R. and M.G. developed the analytical model and prepared the manuscript. All authors revised and approved the final manuscript. All authors declare to have no competing interests. The data supporting the main conclusions of the manuscript are included in the manuscript and appendices. The authors thank Dr. Stephen Starck of the TUM Interactive Editing Service for his language coaching.

APPENDIX A: SUPPLEMENTAL DATA

The mechanism proposed in this paper has been illustrated based on data of a single subject. The same data are shown here for all subjects individually. While we see variability in force and torque magnitudes as expected due to varying weight and style of walking, the key parameters such as event timing (Fig. 8), main actor dynamics (Fig. 9), and torque contributions and resulting dynamics (Fig. 10) remain consistent among subjects. Most importantly, the fit described in Appendix B 4 captures the resulting dynamics that all subjects exhibit in walking. The high variability of push-off timing is visible by the respective vertical lines indicating push-off during mid-stance in some subjects (on average, very early in, e.g., subjects 13 and 16).

APPENDIX B: EQUATION OF MOTION

1. CoP transformation in the sagittal plane

To transform the CoP from the experimentally mandated surface of the force plates into a parallel plane through the optimized rotation point, the intersection between the vector

$$\vec{F} = \vec{R}_{\mathrm{CoP,exp}} + u\,\vec{F}_{\mathrm{GRF}}$$

and the plane

$$\vec{P} = \begin{pmatrix} x_c \\ y_c \\ 0 \end{pmatrix} + v \begin{pmatrix} 1 \\ 0 \\ 0 \end{pmatrix} + w \begin{pmatrix} 0 \\ 0 \\ 1 \end{pmatrix}$$

is calculated: $\vec{F} = \vec{P}$ is solved for the three parameters u, v, and w. During stance, the transformed CoP position equals the intersection point of vector $\vec{F}$ and plane $\vec{P}$, which varies from sample to sample, in terms of the three parameter values (u, v, and w), with the direction of $\vec{F}_{\mathrm{GRF}}$ and the position of $\vec{R}_{\mathrm{CoP,exp}}$ in $\vec{F}$ (Fig. 3, Ref. [20]).

2. Derivation of the single-degree-of-freedom equation of motion

We examine the mechanics of a body with mass m_f (center of mass: CoM) positioned at $\vec{R}_{\mathrm{CoM}}$ and inertia tensor $\mathbf{I}_f$ (for rotations around the CoM). The body is driven by a torque $\vec{\mathcal{T}}$, and it is exposed to gravity, with the vector of acceleration $\vec{g}$, plus two further forces. Generally, the torque $\vec{\mathcal{T}}$ may be any sum of torques applied to the body in addition to the torques resulting from $\vec{F}_{\mathrm{Ank}}$ and $\vec{F}_{\mathrm{GRF}}$ applied through their respective lever arms. As we, here, formulate the equations of motion of only one mechanical body that is, at this stage, not subject to any geometrical constraint, all forces and torques applied to the (free) body are of external character. In the specific biomechanical case that we treat in this study, namely, the dynamics of the human foot contacting the ground, the additional external torque $\vec{\mathcal{T}}$ is exactly the torque transmitted through actuators passing the ankle joint ("Ank"); therefore, we replace right away from hereon the symbol $\vec{\mathcal{T}}$ with $\vec{\mathcal{T}}_{\mathrm{Ank}}$. It should be, yet, always kept in mind, when regarding potential applications of the equations of motion to mechanical situations other then the human foot, that the symbol $\vec{\mathcal{T}}_{\mathrm{Ank}}$ generally represents the sum of all torques acting on the body in addition to those induced by explicitly modeled force vectors through their respective lever arms.

On the one hand, the net vector $\vec{F}_{\mathrm{GRF}}$ of the ground reaction force (GRF) acts at the net position $\vec{R}_{\mathrm{CoP}}$ of the center of pressure (CoP). Describing a force interaction between bodies by a CoP implies that the interaction surface is a plane. Also bear in mind that some $\vec{F}_{\mathrm{GRF}}$ contributions can be of constraint force character. This is actually the case in the model considerations further below, in which a geometric constraint will be introduced: A center of body rotation (CoR) fixed in space. To guarantee consistency of our mechanical body model, while as well including the latter constraint by assuming distributed contact forces ($\vec{F}_{\mathrm{GRF}}$) that act at a net CoP, any such CoP position, whether measured or modeled, must be (re)calculated with respect to a plane that contains the fixed CoR. A CoP position is often determined with respect to the surface of a force platform: say, $\vec{R}_{\mathrm{CoP,exp}}$. Thus, if the CoR is not located exactly in the plane of this surface, then the measured $\vec{R}_{\mathrm{CoP,exp}}$ must be transformed to a plane through the CoR. The transformation condition is that the torque applied by $\vec{F}_{\mathrm{GRF}}$ to the body—i.e., the time rate of change of its moment of momentum around its CoM—is the same, whatever newly chosen (shifted and

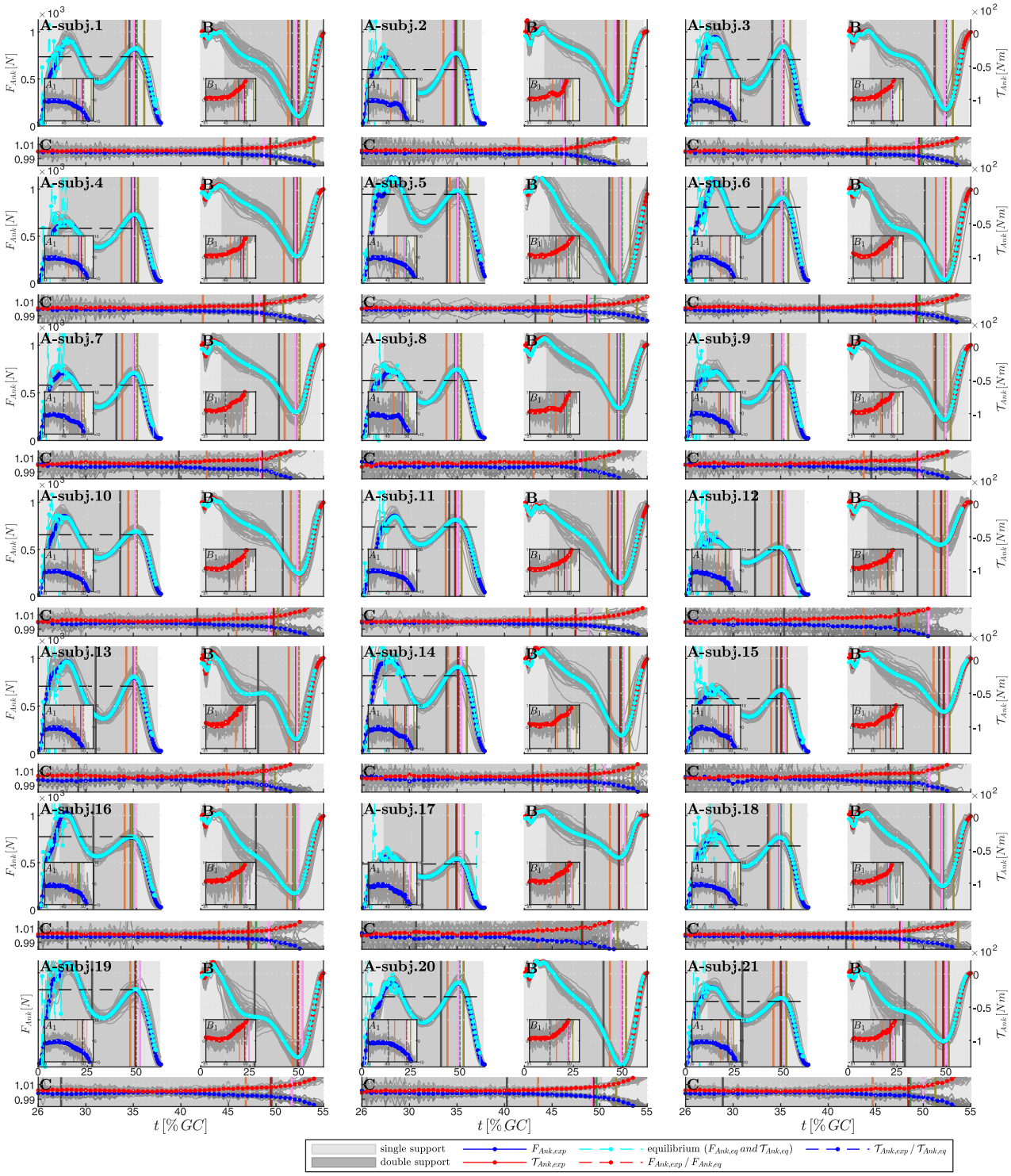

FIG. 9. Main actor dynamics during stance phase for all subjects. Details as shown in Fig. 5 for all 21 subjects. While shapes and magnitudes differ for all subjects, the general dynamics are consistent throughout.

rotated) contact plane: The CoP position $\vec{R}_{\mathrm{CoP}}$ with respect to the newly chosen plane is located where $\vec{F}_{\mathrm{GRF}}$ applied at $\vec{R}_{\mathrm{CoP,exp}}$ intersects the new plane.

On the other hand, the body (foot) is connected to another body (shank) via the joint "Ank" at the position $\vec{R}_{\mathrm{Ank}}$ in space where the (net, resultant, or intersegmental, respectively) joint force $\vec{F}_{\mathrm{Ank}}$ acts on the body. The driving torque $\vec{\mathcal{T}}_{\mathrm{Ank}}$ usually represents a joint torque that is applied on the body via structures surrounding "Ank." However, $\vec{\mathcal{T}}_{\mathrm{Ank}}$ may be even considered an overall torque acting on the body, which consists of the sum of all internally (joint) plus other externally applied torques.

The body's equations of linear motion are

$$m_f\,\ddot{\vec{R}}_{\mathrm{CoM}} = \vec{F}_{\mathrm{GRF}} + \vec{F}_{\mathrm{Ank}} + m_f\,\vec{g}, \tag{B1}$$

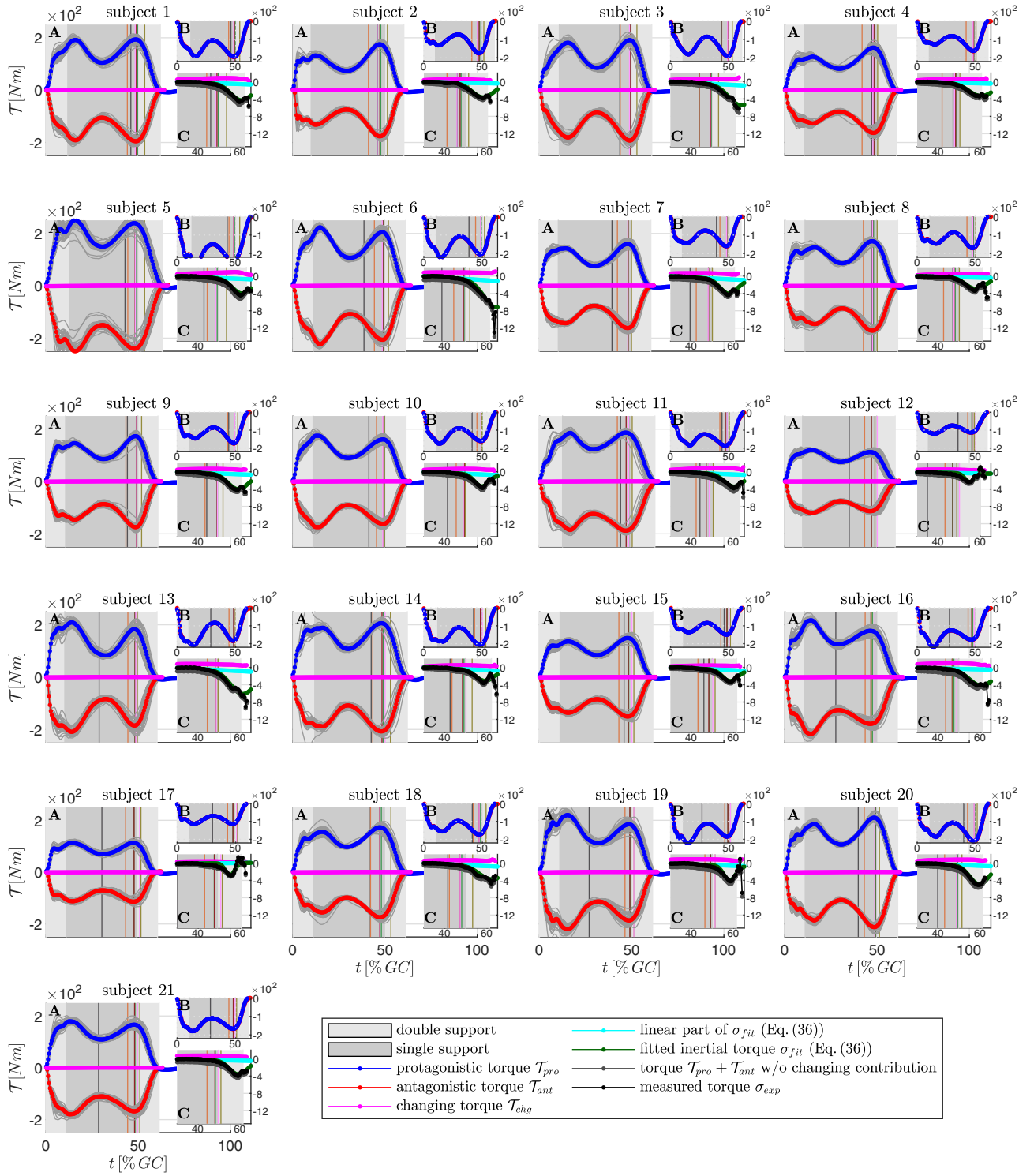

FIG. 10. Three torque contributions according to Eq. (3) for all subjects. Details as shown in Fig. 6 for all 21 subjects. While shapes and magnitudes differ for all subjects, the general dynamics as shown in panels **C** are consistent throughout.

with $\ddot{\vec{R}}_{\mathrm{CoM}}$ symbolizing the vector of the body's linear acceleration in space. As both $\vec{F}_{\mathrm{GRF}}$ and $\vec{F}_{\mathrm{Ank}}$ also cause torques on the body, with their respective lever arms being

$$\vec{r}_{\mathrm{CoP}} = \vec{R}_{\mathrm{CoP}} - \vec{R}_{\mathrm{CoM}} \tag{B2}$$

and

$$\vec{r}_{\mathrm{Ank}} = \vec{R}_{\mathrm{Ank}} - \vec{R}_{\mathrm{CoM}}, \tag{B3}$$

respectively, the body's equations of angular motion write

$$\mathbf{I}_f\,\ddot{\vec{\varphi}} = \vec{\mathcal{T}}_{\mathrm{Ank}} + \vec{r}_{\mathrm{CoP}} \times \vec{F}_{\mathrm{GRF}} + \vec{r}_{\mathrm{Ank}} \times \vec{F}_{\mathrm{Ank}}, \tag{B4}$$

with $\ddot{\vec{\varphi}}$ symbolizing the first time derivative of the vector of the body's angular velocity $\dot{\vec{\varphi}}$ in space, i.e., its angular

acceleration. If we solve the equations of linear motion Eq. (B1) for $\vec{F}_{\rm GRF}$—note that $\vec{F}_{\rm GRF}$ may even contain contributions of a constraint force (see further below)—and insert this in the equations of angular motion Eq. (B4), the latter write

$$\mathbf{I}_f\,\ddot{\vec{\varphi}} = \vec{\mathcal{T}}_{\rm Ank} + (\vec{r}_{\rm Ank} - \vec{r}_{\rm CoP}) \times \vec{F}_{\rm Ank} + m_f\,\vec{r}_{\rm CoP} \times (\ddot{\vec{R}}_{\rm CoM} - \vec{g}). \tag{B5}$$

The vector

$$\vec{R}_{\rm CoM} = \mathfrak{R}_{\rm CoM}\,\vec{e}_r \tag{B6}$$

from the origin to the CoM position (its absolute value is the distance $\mathfrak{R}_{\rm CoM} =: |\vec{R}_{\rm CoM}| \geqslant 0$) can always be written in terms of projections onto the (orthogonal) unit vectors

$$\vec{e}_r = \frac{\vec{R}_{\rm CoM}}{\mathfrak{R}_{\rm CoM}}, \quad \text{note:} \quad \dot{\vec{e}}_r = \dot{\varphi}\,\vec{e}_\varphi\,, \tag{B7}$$

$$\vec{e}_\omega \quad \text{(given or assumed: current axis of rotation)}, \quad \text{note:} \quad \vec{\omega} = \dot{\vec{\varphi}} = \dot{\varphi}\,\vec{e}_\omega\,, \text{ and} \tag{B8}$$

$$\vec{e}_\varphi = \vec{e}_\omega \times \vec{e}_r \quad \text{(constructed)}, \quad \text{note:} \quad \dot{\vec{e}}_\varphi = -\dot{\varphi}\,\vec{e}_r, \tag{B9}$$

of a polar coordinate system for which the location of its origin can be chosen arbitrarily. This coordinate system is right-handed because the triad of its orthonormal vectors $\vec{e}_r$ [Eq. (B7)], $\vec{e}_\varphi$ [Eq. (B9)], and $\vec{e}_\omega$ [Eq. (B8)] is built in the order according to Eq. (B9), which is equivalent to constructing by $\vec{e}_\omega = \vec{e}_r \times \vec{e}_\varphi$ or $\vec{e}_r = \vec{e}_\varphi \times \vec{e}_\omega$, respectively. The symbol $\dot{\varphi}$ in Eq. (B8) is the rate of change (first time derivative) of the scalar (angle) parameter φ around the current axis $\vec{e}_\omega$ of rotation. This axis points in direction $\vec{e}_\omega$ and goes through the origin, with $\vec{\omega} = \dot{\vec{\varphi}}$, thus, symbolizing the vector of the current angular velocity.

By calculating the time derivative of the product in Eq. (B6) and substituting $\dot{\vec{e}}_r$ according to Eq. (B8), we find the CoM velocity

$$\dot{\vec{R}}_{\rm CoM} = \mathfrak{R}_{\rm CoM}\,\dot{\varphi}\,\vec{e}_\varphi + \dot{\mathfrak{R}}_{\rm CoM}\,\vec{e}_r. \tag{B10}$$

The time derivative of Eq. (B10), with multiply using Eqs. (B8) and (B10), then yields the CoM acceleraxtion

$$\ddot{\vec{R}}_{\rm CoM} = (\mathfrak{R}_{\rm CoM}\,\ddot{\varphi} + 2\,\dot{\mathfrak{R}}_{\rm CoM}\,\dot{\varphi})\,\vec{e}_\varphi + (\ddot{\mathfrak{R}}_{\rm CoM} - \mathfrak{R}_{\rm CoM}\,\dot{\varphi}^2)\,\vec{e}_r. \tag{B11}$$

If it is now assumed that the body rotates around a point (the CoR) fixed in space on the axis of rotation ($\vec{e}_\omega$), with the CoR in addition being chosen for (mathematical) convenience to be the origin of the polar coordinate system, while the distance $\mathfrak{R}_{\rm CoM}$ from the origin to CoM is *constrained* by

$$\mathfrak{R}_{\rm CoM} = \text{const.} \tag{B12}$$

to a fixed value (i.e., $\dot{\mathfrak{R}}_{\rm CoM} = \ddot{\mathfrak{R}}_{\rm CoM} = 0$), then Eq. (B11) simplifies, with both the first and the fourth term on its right-hand side vanishing due to this constraint on the body's motion, to

$$\ddot{\vec{R}}_{\rm CoM} = \mathfrak{R}_{\rm CoM}\,(\ddot{\varphi}\,\vec{e}_\varphi - \dot{\varphi}^2\,\vec{e}_r). \tag{B13}$$

That is, the linear acceleration $\ddot{\vec{R}}_{\rm CoM}$ of the CoM is now solely expressed in terms of the angular degrees of freedom that remain due to the constraint expressed in Eq. (B12). Note that introducing this constraint implies $\vec{F}_{\rm GRF}$ to contain the corresponding constraint force contributions.

Next, we see that the time derivative of the angular velocity $\vec{\omega} = \dot{\vec{\varphi}}$ [Eq. (B8)] is simply

$$\ddot{\vec{\varphi}} = \ddot{\varphi}\,\vec{e}_\omega. \tag{B14}$$

Then, substituting Eq. (B14) and the constrained CoM acceleration $\ddot{\vec{R}}_{\rm CoM}$ according to Eq. (B13) in Eq. (B5) allows us to reformulate xthe latter as

$$\ddot{\varphi}\,(\mathbf{I}_f\vec{e}_\omega - m_f\,\mathfrak{R}_{\rm CoM}\,\vec{r}_{\rm CoP} \times \vec{e}_\varphi) = \vec{\mathcal{T}}_{\rm Ank} + (\vec{r}_{\rm Ank} - \vec{r}_{\rm CoP}) \times \vec{F}_{\rm Ank} - m_f\,\vec{r}_{\rm CoP} \times (\dot{\varphi}^2\,\mathfrak{R}_{\rm CoM}\,\vec{e}_r + \vec{g}), \tag{B15}$$

with additionally keeping in mind that we can always write [see Eq. (B9)]

$$\vec{r}_{\rm CoP} \times \vec{e}_\varphi = \vec{r}_{\rm CoP} \times (\vec{e}_\omega \times \vec{e}_r) = (\vec{r}_{\rm CoP}\,\vec{e}_r)\,\vec{e}_\omega - (\vec{r}_{\rm CoP}\,\vec{e}_\omega)\,\vec{e}_r. \tag{B16}$$

If we now restrict ourselves to only considering angular rotations within the x-y plane, i.e., $\vec{e}_\omega = \vec{e}_z$, all force and position vectors introduced so far point perpendicular to $\vec{e}_\omega$, and Eq. (B16) simplifies to

$$\vec{r}_{\rm CoP} \times \vec{e}_\varphi = (\vec{r}_{\rm CoP}\,\vec{e}_r)\,\vec{e}_z. \tag{B17}$$

Next, substituting Eqs. (B2) and (B3), which together imply $\vec{r}_{\rm Ank} - \vec{r}_{\rm CoP} = \vec{R}_{\rm Ank} - \vec{R}_{\rm CoP}$, as well as Eq. (B17) and (B7) into Eq. (B15), plus knowing $\vec{R}_{\rm CoM} \times \vec{R}_{\rm CoM} = 0$, the body's equations of motion Eq. (B15) write

$$\begin{aligned}\ddot{\varphi}(\mathbf{I}_f + m_f\,(\vec{R}_{\rm CoM} - \vec{R}_{\rm CoP})\,\vec{R}_{\rm CoM})\,\vec{e}_z &= \vec{\mathcal{T}}_{\rm Ank} + (\vec{R}_{\rm Ank} - \vec{R}_{\rm CoP}) \times \vec{F}_{\rm Ank} \\ &\quad + m_f\,(\vec{R}_{\rm CoM} - \vec{R}_{\rm CoP}) \times (\dot{\varphi}^2\,\vec{R}_{\rm CoM} + \vec{g}) \\ &= \vec{\mathcal{T}}_{\rm Ank} + (\vec{R}_{\rm Ank} - \vec{R}_{\rm CoP}) \times \vec{F}_{\rm Ank} \\ &\quad + m_f\,(\vec{R}_{\rm CoM} - \vec{R}_{\rm CoP}) \times \vec{g} \\ &\quad + m_f\,\dot{\varphi}^2\,\vec{R}_{\rm CoM} \times \vec{R}_{\rm CoP}.\end{aligned} \tag{B18}$$

If we further assumed the constraint force acting in the CoR fixed at the origin to be the only contribution to $\vec{F}_{\rm GRF}$, with $\vec{R}_{\rm CoP} = 0$ implying $\vec{r}_{\rm CoP} = -\vec{R}_{\rm CoM}$ [Eq. (B2)], then the specific form Eq. (B18) of the body's equations of motion Eq. (B15) would contract to

$$\ddot{\varphi}(\mathbf{I}_f + m_f\,\vec{R}_{\rm CoM}\,\vec{R}_{\rm CoM})\,\vec{e}_z = \vec{\mathcal{T}}_{\rm Ank} + \vec{R}_{\rm Ank} \times \vec{F}_{\rm Ank} + m_f\,\vec{R}_{\rm CoM} \times \vec{g}. \tag{B19}$$

Sticking, however, to the consideration of distributed contact forces that are transmitted at a plane, which is properly described by a CoP, we can still further simplify Eq. (B18), while not losing a lot of substance. Namely, if it is eventually assumed that $\vec{F}_{\rm Ank}$ acts within the sagittal (x-y) plane, just like

the gravitational acceleration $\vec{g}$ for which we assume

$$\vec{g} = \begin{pmatrix} 0 \\ -g \\ 0 \end{pmatrix} \tag{B20}$$

here, and the torque $\vec{\mathcal{T}}_{\text{Ank}}$ points perpendicular to the sagittal plane (solely a z component), we end up with just one equation of motion: only the z component of Eq. (B18) [or Eq. (B19), respectively] remains, which lets us write Eq. (B18) the following way:

$$\begin{aligned} &\ddot{\varphi}(I_{f,z} + m_f\,(\vec{R}_{\text{CoM}} - \vec{R}_{\text{CoP}})\,\vec{R}_{\text{CoM}}) \\ &:= \ddot{\varphi}\,I_{f,\text{CoR}} \\ &= \mathcal{T}_{\text{Ank},z} + [(\vec{R}_{\text{Ank}} - \vec{R}_{\text{CoP}}) \times \vec{F}_{\text{Ank}}]_z \\ &\quad - m_{fx}\,g\,(R_{\text{CoM},x} - R_{\text{CoP},x}) \\ &\quad + m_f\,\dot{\varphi}^2\,[\vec{R}_{\text{CoM}} \times \vec{R}_{\text{CoP}}]_z, \end{aligned} \tag{B21}$$

with $I_{f,z} = [\mathbf{I}_f\,\vec{e}_z]_z$ symbolizing the moment of inertia of the body (foot) for rotation in the x-y-plane around its CoM. In a human foot's contact phase during walking, it turns out that the contribution caused by the *centrifugal force*, the last term on the right-hand side of Eq. (B21), is perfectly *negligible*. For our planar model, force components in the z-axis direction do not contribute to the torque in the sagittal plane and are thus set to zero. This lets us write Eq. (B21) as

$$\begin{aligned} \ddot{\varphi} I_{f,\text{CoR}} = \mathcal{T}_{\text{Ank},z} &+ \left[\begin{pmatrix} R_{\text{Ank},x} \\ R_{\text{Ank},y} \\ 0 \end{pmatrix} \times \begin{pmatrix} F_{\text{Ank},x} \\ F_{\text{Ank},y} \\ 0 \end{pmatrix} \right]_z \\ &- m_f\,g\,(R_{\text{CoM},x} - R_{\text{CoP},x}) \\ &- \left[\begin{pmatrix} R_{\text{CoP},x} \\ 0 \\ 0 \end{pmatrix} \times \begin{pmatrix} F_{\text{Ank},x} \\ F_{\text{Ank},y} \\ 0 \end{pmatrix} \right]_z. \end{aligned} \tag{B22}$$

This compactifies further by expressing Eq. (B22) explicitly in terms of vector components in the sagittal plane, i.e.,

$$\begin{aligned} \ddot{\varphi} I_{f,\text{CoR}} &= \mathcal{T}_{\text{Ank}} + R_{\text{Ank},x}\,F_{\text{Ank},y} - R_{\text{CoM},x}\,m_f\,g \\ &\quad - R_{\text{Ank},y}\,F_{\text{Ank},x} - R_{\text{CoP},x}\,(F_{\text{Ank},y} - m_f\,g) \\ &= \underbrace{-F_{\text{Ank}}\,\mathcal{R}_{F_{\text{Ank}}}}_{\text{antagonist}} - \underbrace{\mathcal{R}_g\,m_f\,g}_{\text{changing}} + \underbrace{\mathcal{T}_{\text{Ank}} - R_{\text{CoP},x}\,F_{\text{Ank},y}}_{\text{protagonist}}, \end{aligned} \tag{B23}$$

abbreviating $\mathcal{T}_{\text{Ank},z}$ with $\mathcal{T}_{\text{Ank}}$ as well as the norm of the projected force $|\vec{F}_{\text{Ank}}|$ with F_{Ank} and defining

$$\mathcal{R}_g = R_{\text{CoM},x} - R_{\text{CoP},x}, \tag{B24}$$

$$\mathcal{R}_{F_{\text{Ank}}} = R_{\text{Ank},x}\,\cos\alpha_F + R_{\text{Ank},y}\,\sin\alpha_F, \tag{B25}$$

$$\begin{aligned} \mathcal{R} &= (R_{\text{Ank},x} - R_{\text{CoP},x})\,\cos\alpha_F + R_{\text{Ank},y}\,\sin\alpha_F \\ &= \mathcal{R}_{F_{\text{Ank}}} - R_{\text{CoP},x}\,\cos\alpha_F. \end{aligned} \tag{B26}$$

For brevity we introduce the symbol σ for the left-hand side of Eq. (B23):

$$\sigma = \ddot{\varphi}\,I_{f,\text{CoR}}, \tag{B27}$$

and $\sigma = 0$ indicates equilibrium.

3. Center of pressure (CoP)

Equation (B23) can be solved for $R_{\text{CoP},x}$ as

$$\begin{aligned} R_{\text{CoP},x} &= \frac{R_{\text{Ank},x}\,F_{\text{Ank},y} - R_{\text{Ank},y}\,F_{\text{Ank},x}}{F_{\text{Ank},y} - m_f\,g} \\ &\quad + \frac{-R_{\text{CoM},x}\,m_f\,g + \mathcal{T}_{\text{Ank}} - \ddot{\varphi}\,I_{f,\text{CoR}}}{F_{\text{Ank},y} - m_f\,g} \\ &= \frac{\mathcal{R}_{F_{\text{Ank}}}\,|\vec{F}_{\text{Ank}}| + R_{\text{CoM},x}\,m_f\,g - \mathcal{T}_{\text{Ank}} + \sigma}{|\vec{F}_{\text{Ank}}|\,\cos\alpha_F + m_f\,g}. \end{aligned} \tag{B28}$$

This equation explicitly describes the influence of each individual dynamical actor on the positioning of the CoP traveling in the ground plane. The influence of $\vec{F}_{\text{Ank}}$ can be divided into two effects. The vertical component is moving the CoP posteriorly as it increases the $\vec{F}_{\text{Ank}}$ magnitude. The horizontal component, while having a substantially smaller impact as it changes direction during stance phase initially pushes the CoP slightly anteriorly while contributing to a posteriorly shift during the second half of stance.

The ankle torque shifts the CoP anteriorly but all shifts are always in relation to the primary antagonistic actor $F_{\text{Ank},y} - m_f\,g$. Setting the inertial torque $\ddot{\varphi}\,I_{f,\text{CoR}}$ [Eqs. (B23), (B27)] to zero determines the position of a CoP position to keep equilibrium for any given load situation. The comparison of this equilibrium position with the experimental CoP trajectory reveals at what instant the foot leaves its equilibrium (Fig. 7).

The CoP keeps an equilibrium configuration while traveling until fairly late in stance. Due to the tumbling ankle force (Fig. 5, bottom, and Fig. 9 for all subjects), which cannot keep the CoP in equilibrium, and the still building ankle torque (see chronological order, especially $t_{\min(\mathcal{T}_{\text{Ank}})} - t_{\max(F_{\text{Ank}})}$ in Fig. 8), which pushes the theoretical equilibrium CoP more anteriorly, the actual experimental CoP cannot follow suit, falls behind its equilibrium position, and, as a result, the inertial torque (σ) accelerates the heel upwards and dynamically rotates the foot in forward direction.

4. Fitting σ

For data analysis we have fitted the experimental foot torque data with a composite function: the equilibrium phase starting with the onset of negative ankle torque can be well described by a linear function (creep) while the explosive foot rotation (push-off) shows a consistent exponential characteristic [Fig. 6(C)], well described by a Gaussian function,

$$\sigma_{\text{fit}}(t) = \underbrace{a_1\,t + a_2}_{\text{linear}} + \underbrace{a_3\,\exp\left[-\frac{(t-a_4)^2}{a_5^2}\right]}_{\text{Gaussian}}, \tag{B29}$$

with $a_{1\text{-}5}$ denoting the parameters of the fitted function and t being the time in % gait cycle (GC). Thus, the function for which the optimizer minimizes the sum of squares ($\sum_i f(t_i)^2$) to determine the fit parameters is

$$f(t) = \sigma_{\text{fit}}(t) - \sigma_{\text{exp}}(t), \tag{B30}$$

with σ_{exp} symbolizing the measured inertial foot torque, determined by evaluating the right-hand side of Eq. (B23). The optimization problem $\min[\sum_i f(t_i)^2]$ has been implemented

in MATLAB2020b using *lsqnonlin*. The resulting parameters a_3, a_4, and a_5 characterise the height, peak time, and bell width, respectively. The step-specific average residual

$$\epsilon = \sqrt{\frac{1}{N}\sum_{i=1}^{N} f(t_i)^2} \tag{B31}$$

quantifies the quality of the resulting fit. For each step, this allows us to determine the onset of the exponential growth in torque as the instance in time when the Gaussian function part exceeds the residual

$$a_3 \exp\left[-\frac{(t_\epsilon - a_4)^2}{a_5^2}\right] - \epsilon = 0. \tag{B32}$$

t_ϵ is reported as the onset of foot rotation at the very end of the single support phase.

APPENDIX C: EVENT TIMING

Events of importance during the gait cycle have been identified and calculated from experimental data to determine their succession. This has been done for each analyzed step separately. Below, the calculation of each event is described.

1. Touchdown t_{TD}

The events of the ipsi- and contralateral legs' vertical GRF components exceeding 20 N determine the touchdown instants t_{TD} (begin of stance) and t_{TDc} (begin final double support), respectively.

2. Takeoff t_{TO}

The events of the contra- and ipsilateral legs' vertical GRF components falling below 20 N determine the end of initial double support (t_{TOc}) and of stance (t_{TO}), respectively.

3. Push-off onset $t_{\text{push-off}}$

Push-off describes the phase of positive power output at the ankle joint [43]. The onset of push-off is defined as the instance in time the ankle power turns from negative to positive before exhibiting a positive power peak in late stance.

The commonly accepted kinematics in biomechanics textbooks, e.g., Ref. [44], describes ankle dorsiflexion throughout mid-stance and plantarflexion in terminal stance. The change in movement direction results in a coincidental sign change in ankle power at which instant a maximum amount of energy is stored in the Achilles tendon. This process ideally exhibits a smooth power curve with a single zero-crossing in late stance.

In our data, however, we observed stepping patterns with very early plantarflexion as an occasional occurrence in some subjects and regular patterns, as described above, in others. Early plantarflexion results in an early zero-crossing of the power curve and leaves the ankle power hovering close to the abscissa. To reliably determine the instant of push-off, we shifted the threshold for detecting positive power output from zero to 5% of the power maximum. Accordingly, push-off onset is defined as the instant ($t_{\text{push-off}}$) the ankle power exceeds this threshold before reaching its maximum.

4. Ankle force exceeds proximal body weight $t_{F>m_p g}$

The instance in time ($t_{F>m_p g}$) the ankle force exceeds the body weight ($m_p g$) of all segments proximal to the foot on the ground ($m_p = M - m_f$; M is the overall body mass) is determined by the first sample at which the norm of the ankle force $\vec{F}_{\mathrm{Ank}}$ exceeds the remaining body's weight (m_p) for the first time after the norm's minimum during midstance in single support.

5. Ankle force maximum $t_{\max(F_{\mathrm{Ank}})}$

The instance of the ankle force maximum [$t_{\max}(F_{\mathrm{Ank}})$] is determined by the sample the ankle force norm ($|\vec{F}_{\mathrm{Ank}}|$) reaches its maximum value after having passed its minimum in single support.

6. Ankle torque minimum $t_{\min(\mathcal{T}_{\mathrm{Ank}})}$

The ankle torque shows a monotonous decrease during single support. The instance of ankle torque minimum [$t_{\min}(\mathcal{T}_{\mathrm{Ank}})$] is defined as the sample of the torque's smallest value after having become consistently negative in single support.

7. Loss of equilibrium t_ϵ

This instant has been defined using the fit described in Appendix B 4. The exponentially increasing inertial torque σ is indicative of the foot losing its equilibrium and beginning to rotate forcefully into swing. Accounting for indeterminacy of the fit due to measurement error, we use the residual ϵ according to Eq. (B31) for calculating the instant of loss in equilibrium (t_ϵ) defined as the sample the Gaussian function exceeds ϵ, i.e., deviates by ϵ from the linear term of the function given in Eq. (B29).

8. Launching phase onset t_{launch}

The occurrence of the maximum ankle jerk $\dddot{\varphi}_{\mathrm{Ank}}$ defines the onset of the launching phase [26].

[1] L. Klenerman and B. Wood, *The Human Foot: A Companion to Clinical Studies* (Springer Science & Business Media, Cham, 2006).

[2] R. M. Alexander, Bipedal animals, and their differences from humans, J. Anat. **204**, 321 (2004).

[3] C. Lee and C. Farley, Determinants of the center of mass trajectory in human walking and running, J. Experim. Biol. **201**, 2935 (1998).

[4] M. A. Cairns, R. G. Burdett, J. C. Pisciotta, and S. R. Simon, A biomechanical analysis of racewalking gait, Med. Sci. Sports Exer. **18**, 446 (1986).

[5] K. Steudel-Numbers and C. Wall-Scheffler, Optimal running speed and the evolution of hominin hunting strategies, J. Hum. Evol. **56**, 355 (2009).

[6] H. Geyer, A. Seyfarth, and R. Blickhan, Spring-mass running: simple approximate solution and

application to gait stability, J. Theor. Biol. **232**, 315 (2005).

[7] S. W. Lipfert, M. Günther, D. Renjewski, S. Grimmer, and A. Seyfarth, A model-experiment comparison of system dynamics for human walking and running, J. Theor. Biol. **292**, 11 (2012).

[8] D. Sutherland, L. Cooper, and D. Daniel, The role of the ankle plantar flexors in normal walking, J. Bone Joint Surg. **62**, 354 (1980).

[9] A. Bähler, The biomechanics of the foot, Clin. Prosth. Ortho. **10**, 8 (1986).

[10] S. H. Scott and D. A. Winter, Biomechanical model of the human foot: kinematics and kinetics during the stance phase of walking, J. Biomech. **26**, 1091 (1993).

[11] P. O. McKeon, J. Hertel, D. Bramble, and I. Davis, The foot core system: a new paradigm for understanding intrinsic foot muscle function, British J. Sports Med. **49**, 290 (2015).

[12] S. Davis and D. G. Caldwell, The design of an anthropomorphic dexterous humanoid foot, *Proceedings of the EEE/RSJ International Conference on Intelligent Robots and Systems (IROS'10)*, pp. 2200–2205 (2010).

[13] N. B. Holowka and D. E. Lieberman, Rethinking the evolution of the human foot: insights from experimental research, J. Exp. Biol. **221**, jeb174425 (2018).

[14] S. Bullimore and J. Burn, Consequences of forward translation of the point of force application for the mechanics of running, J. Theor. Biol. **238**, 211 (2006).

[15] R. F. Ker, M. B. Bennett, S. R. Bibby, R. C. Kester, and R. M. Alexander, The spring in the arch of the human foot, Nature (London) **325**, 147 (1987).

[16] E. P. Salathé, G. A. Arangio, and E. P. Salathé, The foot as a shock absorber, J. Biomech. **23**, 655 (1990).

[17] N. Messenger, Moving the human machine: understanding the mechanical characteristics of normal human walking, Phys. Educ. **29**, 352 (1994).

[18] J. Donelan, R. Kram, and A. Kuo, Mechanical and metabolic determinants of the preferred step width in human walking, Proc. R. Soc. London B **268**, 1985 (2001).

[19] J. P. Charles, B. Grant, K. D'Août, and K. T. Bates, Foot anatomy, walking energetics, and the evolution of human bipedalism, J. Human Evolution **156**, 103014 (2021).

[20] D. Renjewski, S. Lipfert, and M. Günther, The foot in walking - towards developing a constrained model of stance phase dynamics, in *Proceedings of the ASME 2022 International Design Engineering Technical Conferences and Computers and Information in Engineering Conference, Volume 9: 18th International Conference on Multibody Systems, Nonlinear Dynamics, and Control (MSNDC)* (ASME, 2022), Paper No. DETC2022-89185.

[21] S. W. Lipfert, *Kinematic and Dynamic Similarities between Walking and Running* (Verlag Dr. Kovač, Hamburg, 2010).

[22] NASA, Anthropometric Source Book, Tech. Rep. 1024, I-III, NASA Scientific and Technical Information Office (1978).

[23] U. Hahn, Entwicklung mehrgliedriger Modelle zur realistischen Simulation dynamischer Prozesse in biologischen Systemen, Diplomathesis, Eberhard-Karls-Universität, Tübingen (1993), https://biomechanicsbiorobotics.info/tatbiomechanik/publ/dipl/ulihahn/diplom_uli_hahn.pdf.

[24] S. W. Lipfert, M. Günther, and A. Seyfarth, Diverging times in movement analysis, J. Biomech. **42**, 786 (2009).

[25] M. Günther, V. A. Sholukha, D. Keßler, V. Wank, and R. Blickhan, Dealing with skin motion and wobbling masses in inverse dynamics, J. Mech. Med. Biol. **3**, 309 (2003).

[26] S. W. Lipfert, M. Günther, D. Renjewski, and A. Seyfarth, Impulsive ankle push-off powers leg swing in human walking, J. Exp. Biol. **217**, 1218 (2014).

[27] D. A. Winter, Biomechanics and Motor Control of Human Movement, *Biomechanics and Motor Control of Human Movement* (John Wiley & Sons, New York, NY, 2009).

[28] See Supplemental Material at http://link.aps.org/supplemental/10.1103/PhysRevE.106.064405 for accompanying video containing a visualization of the method to derive the velocity pole of the foot.

[29] N. J. Cronin, B. I. Prilutsky, G. A. Lichtwark, and H. Maas, Does ankle joint power reflect type of muscle action of soleus and gastrocnemius during walking in cats and humans? J. Biomech. **46**, 1383 (2013).

[30] J. M. Morawski, A simple model of step control in bipedal locomotion, IEEE Trans. Biomed. Eng. **BME-25**, 544 (1978).

[31] G. Cavagna, H. Thys, and A. Zamboni, The sources of external work in level walking and running, J. Physiol. **262**, 639 (1976).

[32] H. Geyer, A. Seyfarth, and R. Blickhan, Compliant leg behaviour explains basic dynamics of walking and running, Proc. R. Soc. London B **273**, 2861 (2006).

[33] R. Blickhan, The spring-mass model for running and hopping, J. Biomech. **22**, 1217 (1989).

[34] B. R. Whittington and D. G. Thelen, A simple mass-spring model with roller feet can induce the ground reactions observed in human walking, J. Biomech. Eng. **131**, 011013 (2009).

[35] C. Taylor, N. Heglund, T. McMahon, and T. Looney, Energetic cost of generating muscular force during running: A comparison of large and small animals, J. Exp. Biol. **86**, 9 (1980).

[36] C. Taylor, Force development during sustained locomotion: A determinant of gait, speed and metabolic power, J. Exp. Biol. **115**, 253 (1985).

[37] R. Kram and C. Taylor, Energetics of running: A new perspective, Nature (London) **346**, 265 (1990).

[38] R. Blickhan, A. Seyfarth, H. Geyer, S. Grimmer, H. Wagner, and M. Günther, Intelligence by mechanics, Philos. Trans. R. Soc. A **365**, 199 (2007).

[39] D. F. B. Haeufle, I. Wochner, D. Holzmüller, D. Driess, M. Günther, and S. Schmitt, Muscles reduce neuronal information load: Quantification of control effort in biological vs. robotic pointing and walking, Front. Robot. AI **7**, 77 (2020).

[40] A. Seyfarth, H. Geyer, and H. Herr, Swing-leg retraction: a simple control model for stable running, J. Exp. Biol. **206**, 2547 (2003).

[41] M. Wisse, C. G. Atkeson, and D. K. Kloimwieder, Swing leg retraction helps biped walking stability, in *Proceedings of the 5th IEEE-RAS International Conference on Humanoid Robots* (IEEE, Piscataway, NJ, 2005), pp. 295–300.

[42] L. Liebenberg, Persistence hunting by modern huntergatherers, Curr. Anthropol. **47**, 1017 (2006).

[43] A. Salih and S. Ibrahim, Comparative Kinesiology of the Human Body: Normal and Pathological, *Comparative Kinesiology of the Human Body: Normal and Pathological Conditions* (Academic Press, San Diego, CA, 2020).

[44] J. Perry and J. M. Burnfield, *Gait Analysis: Normal and Pathological Function*, 2nd ed. (Slack Books, California, 2010).